Supporting Information
for

Solar light-assisted electrochemical CO_2 reduction on boron-doped diamond cathode

Goki Iwai[1], Andrea Fiorani[1], Chiaki Terashima[2] and Yasuaki Einaga[1]*

1. Department of Chemistry, Keio University, Yokohama 223-8522, Japan.
2. Research Center for Space System Innovation, Research Institute for Science and Technology, Tokyo University of Science, Yamazaki, Noda, 278-8510, Japan.

Table of content

1. Boron-doped diamond: SEM micrograph and Raman spectrum

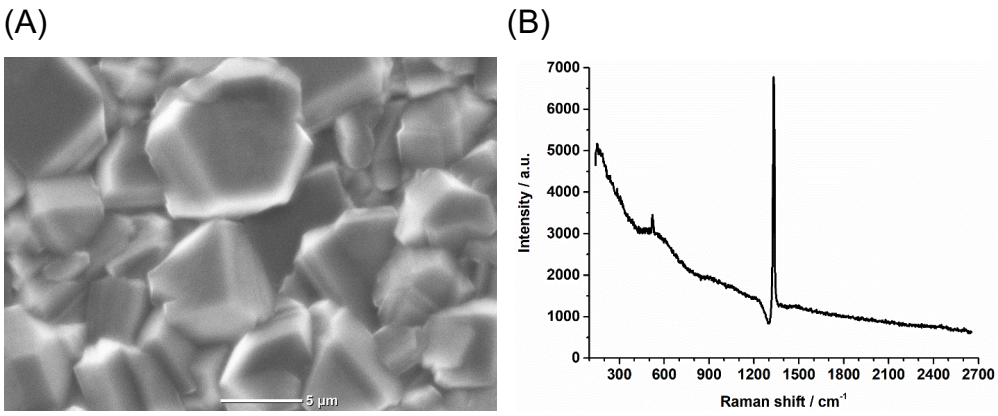

Fig. S1 (a) SEM image of fabricated BDD showing polycrystalline structure of micrometre grain size; (b) Raman spectrum showing diamond phonon at 1332 cm^{-1}, and two weak peaks (500 and 1200 cm^{-1}) as result of boron doping (B/C 0.1 %). A peak around 1530 cm^{-1} (G band) is not evident which indicates the absence of sp^2 carbon.

2. α-Fe_2O_3: characterisation

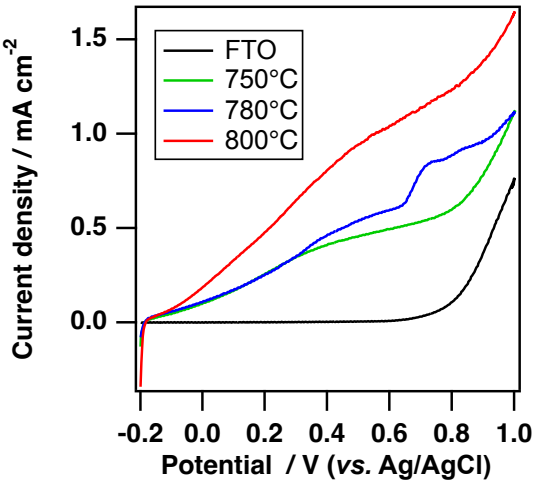

Fig. S2 Characterisation of fabricated α-Fe_2O_3 with different heat treatment temperature. Photoelectrochemical response measured by cyclic voltammetry at 100 mV s^{-1} in 0.5 M KOH with 1 sun light applied (AM 1.5, 100 mW cm^{-2}). Reference electrode: Ag/AgCl/KCl (sat'd).

Table S1 Comparison of current for α-Fe_2O_3 at 1.23 V vs. RHE under 1 Sun / AM1.5 illumination.

Electrolyte	Current density / mA cm^{-2}	Ref.
1 M NaOH (pH 13.6)	1.24 mA cm^{-2}	1
1 M NaOH	1.26 mA cm^{-2}	2
1 M NaOH (pH 13.6)	0.86 mA cm^{-2}	3
1 M NaOH (pH 13.6)	0.61 mA cm^{-2}	4
1 M NaOH (pH 13.6)	0.43 mA cm^{-2}	5
0.5 M KOH	0.59 mA cm^{-2}	This work

3. TiO_2 NT: characterisation

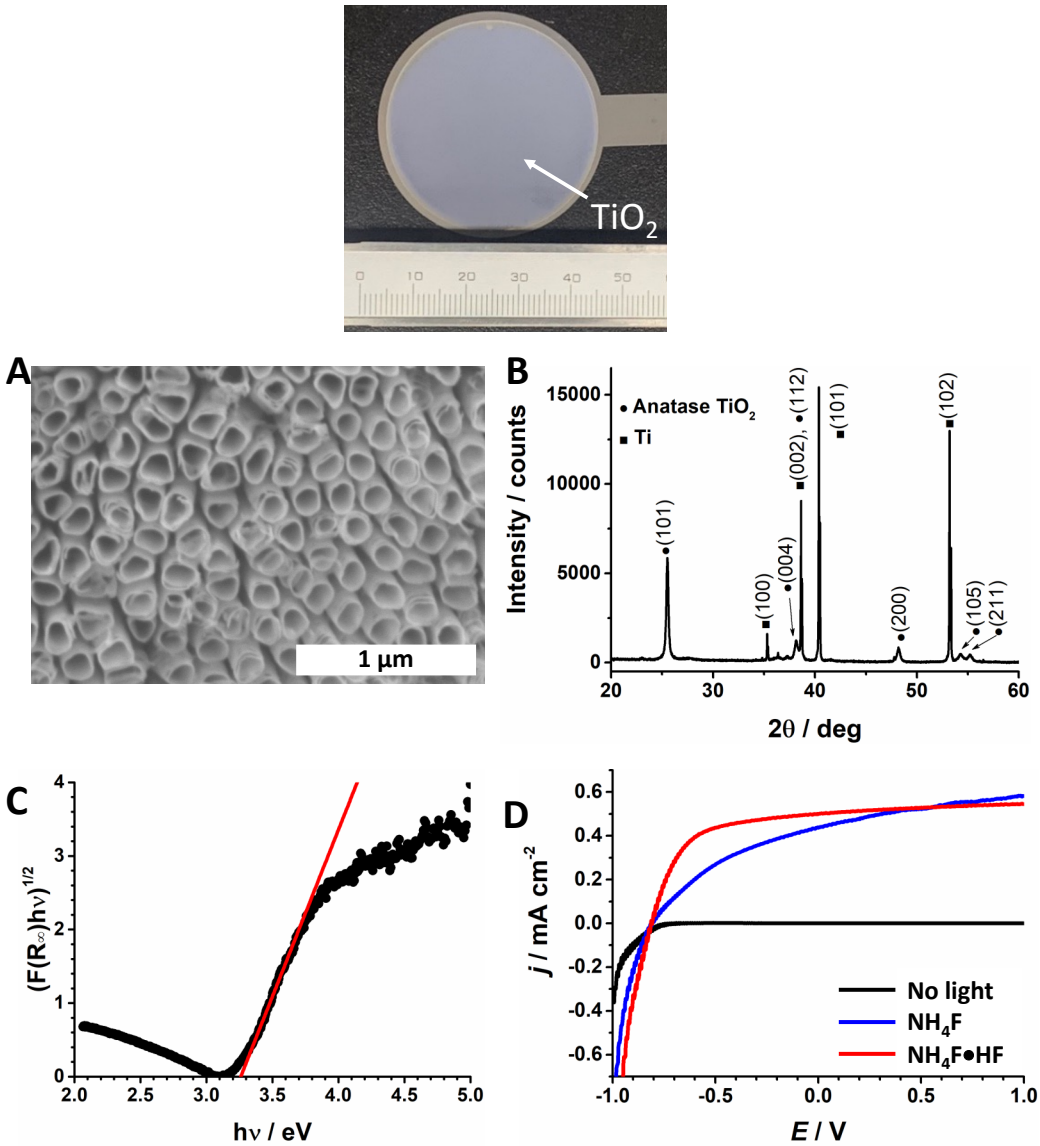

Fig. S3 Photograph of fabricated TiO_2 NT electrode; Characterisation of TiO_2 NT. A) SEM micrograph, scale bar is 1 µm. B) XRD spectrum. C) Kubelka-Munk plot. D) Photoelectrochemical response measured by cyclic voltammetry at 100 mV s^{-1} in 0.5 M KOH with light applied 6.5 mW cm^{-2}.for TiO_2 NT fabricated with NH_4F (blue) or NH_4F•HF (red and black). Reference electrode: Ag/AgCl/KCl (sat'd). Reproduced from Ref. 6 with permission from the Royal Society of Chemistry.

4. Electrochemical CO_2 reduction (Pt-BDD)

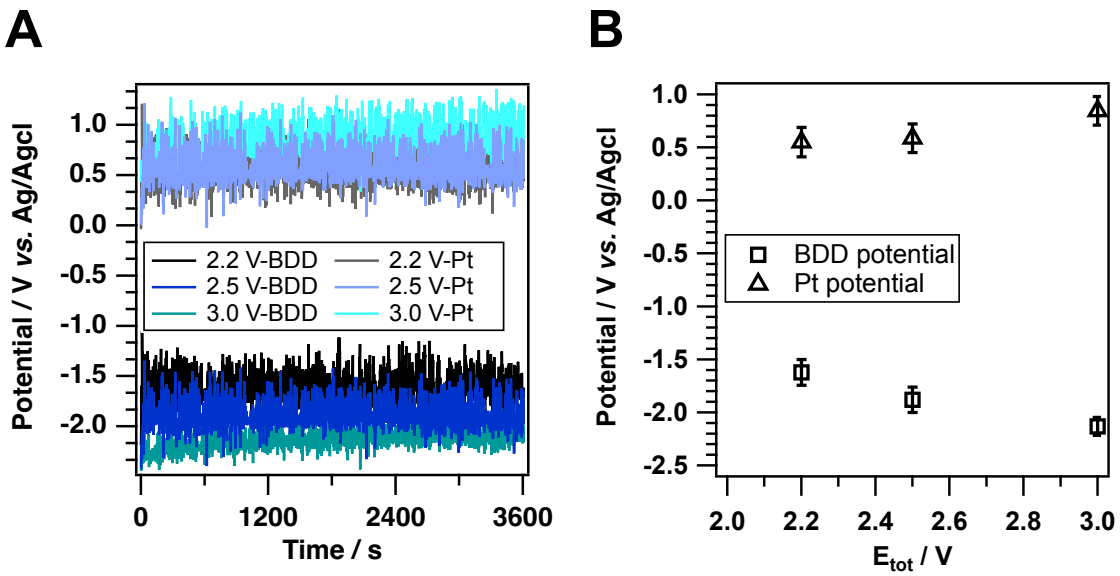

Fig. S4 Potential for BDD and Pt electrode, respectively, during CO_2 reduction (without light irradiation). A) Measured potential during the total fixed voltage CO_2 reduction between BDD cathode and Pt anode for 60 min. B) The average value and standard deviation of the measured potential reported in Fig. A.

Table S2 Faradaic efficiency and ECE for CO_2 reduction without light irradiation.
Total applied voltage fixed between BDD cathode and Pt anode for 60 min.

Applied voltage / V	FE_{HCOOH} / %	ECE / %
2.2	-	-
2.5	50	28
3.0	75	35

※ FE: Faradaic efficiency for formic acid
※ ECE: Electrical-to-chemical energy conversion efficiency for formic acid

Table S3 Faradaic efficiency for CO_2 reduction without light irradiation.
Total applied voltage fixed between the BDD cathode vs the reference electrode for 60 min.

Applied potential / V *vs.* Ag/AgCl/KCl (sat'd)	HCOOH / %
2.2	66.3±4.8
2.3	72.0±3.6
2.4	74.0±0.8

5. BDD cathode and α-Fe_2O_3 photoanode

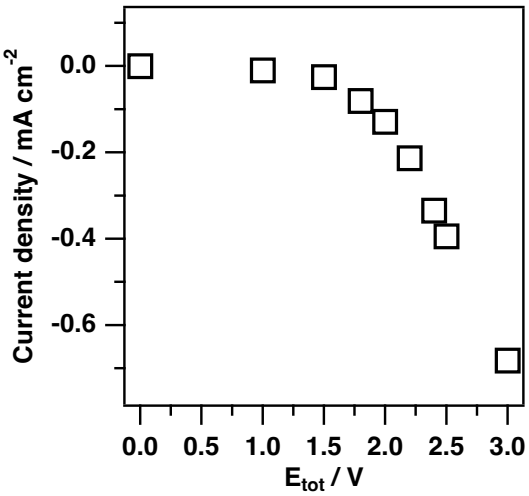

Fig. S5 Current density during CO_2 reduction with BDD cathode and α-Fe_2O_3 photoanode under 1-sun illumination as function of total cell voltage, from 1 V to 3.0 V applied for 15 min.

6. Photoelectrochemical CO_2 reduction (α-Fe_2O_3-BDD)

Table S4 Faradaic efficiencies for all the products from photoelectrochemical CO_2 reduction

E_{tot} / V	HCOOH / %	H_2 / %	CO / %	Total / %
2.0	58.9±3.8	61.9±10.0	2.6±0.1	98.8±2.1
2.2	62.2±4.4	34.3±8.4	2.4±0.4	104.4±8.2
2.4	58.9±13.1	35.3±14.3	1.6±0.5	101±5.3
2.5	58.8±3.8	39.9±3.9	1.8±0.1	101±0.1

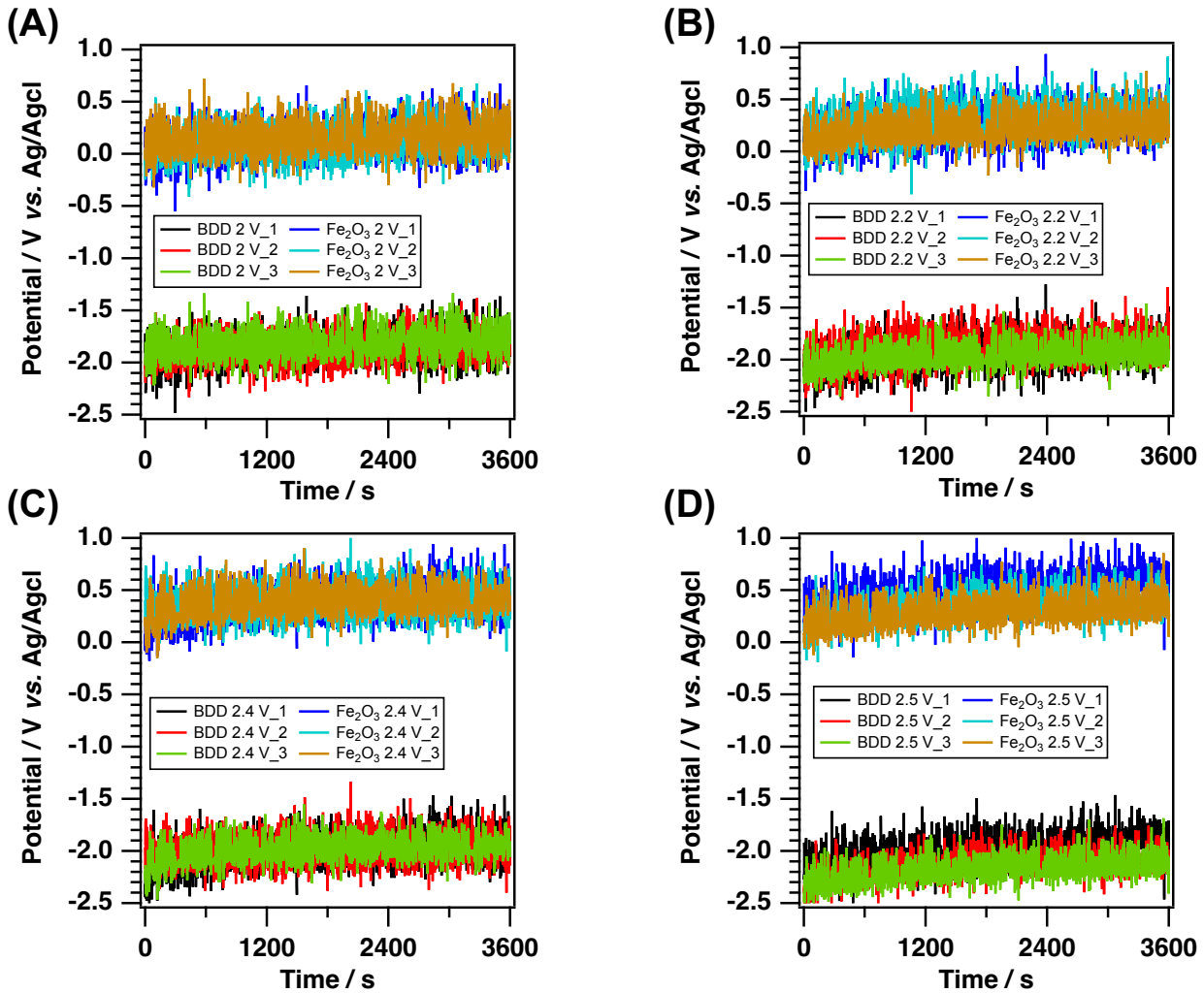

Fig. S6 Potential monitoring: potential of BDD cathode and Fe_2O_3 anode during the photoelectrochemical CO_2 reduction. (A) 2.0 V, (B) 2.2 V, (C) 2.4 V, (D) 2.5 V.

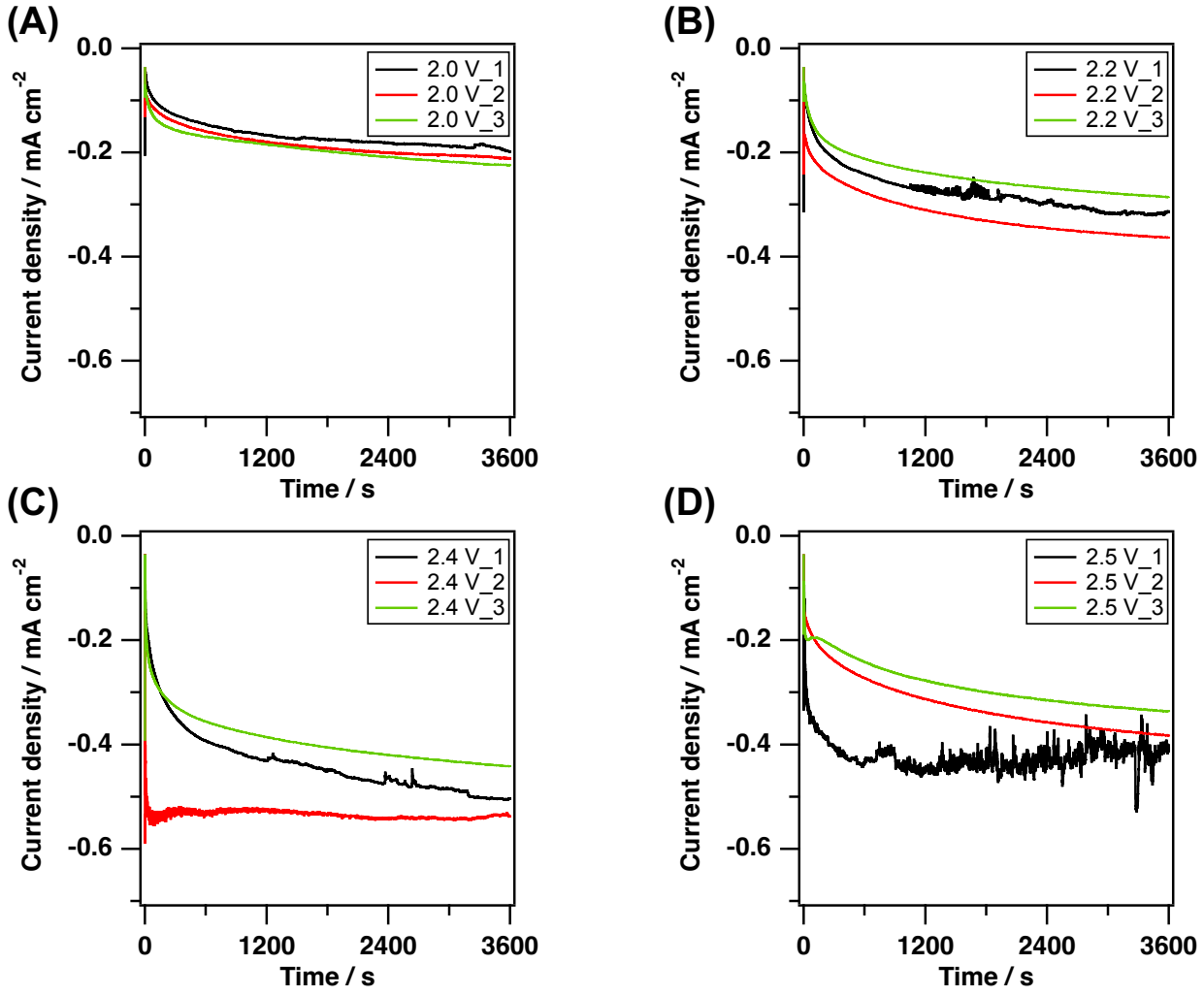

Fig. S7 Current density during the photoelectrochemical CO_2 reduction. (A) 2.0 V, (B) 2.2 V, (C) 2.4 V, (D) 2.5 V

7. Potential distribution (TiO_2 NT-BDD)

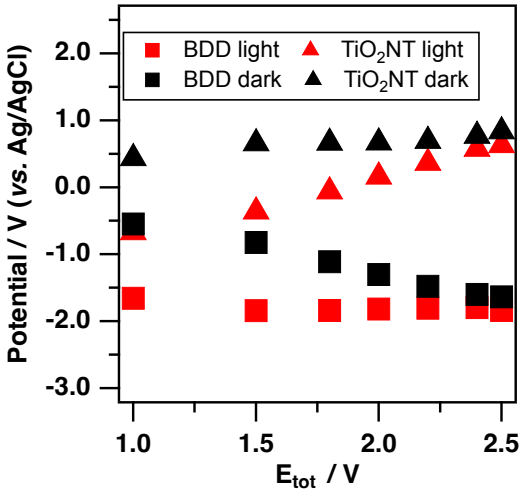

Fig. S8 Potential distribution for TiO_2 NT photoanode and BDD cathode as function of applied total potential. CO_2 reduction for 15 min, with 1-sun irradiation (red), and dark (black).

8. Current of α-Fe_2O_3-BDD and α-Fe_2O_3 photoelectrochemical systems

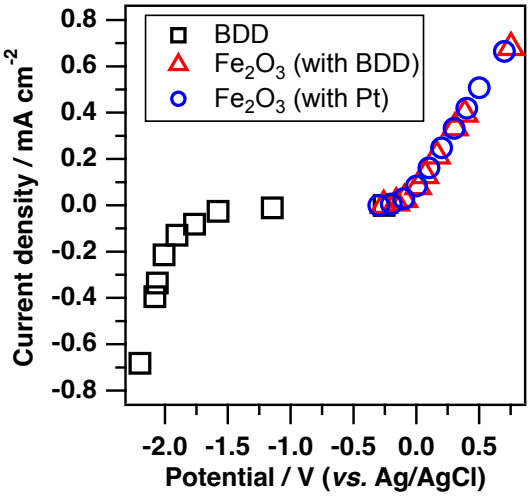

Fig. S9 Current density as function of potential measured at BDD cathode (black square) and α-Fe_2O_3 photoanode (red triangle) during CO_2 reduction under 1 sun illumination applying total fixed potential between BDD cathode and α-Fe_2O_3 photoanode.
Current density as function of potential measured at α-Fe_2O_3 photoanode (with Pt counter electrode) during water oxidation in 0.5 M NaOH under 1-sun illumination (blue circle). Reference electrode: Ag/AgCl/KCl (sat'd).
The Pt counter electrode (12.6 cm^2) is used to assure that the only limiting reaction is the photoelectrochemical water oxidation at α-Fe_2O_3 photoanode (2.8 cm^2).

9. Comparison with other solar light-assisted systems

Table S5 Comparison of FE, current density (j), η_{PAE} and η_{ECE} with other solar light-assisted systems for CO_2 reduction, comprising different anode and cathode couples.

System	Anode	Cathode	FE	j / mA cm^{-2}	η_{PAE}	η_{ECE}	Ref.
PEC	GaAs/ InGaP/TiO_2/Ni	Pd/C-Ti mesh	94% (HCOOH)	8.5	10%	59.3%	7
PV + EC	IrO_2 Nanotubes	Cu-Ag Nanocoral	70% (CO/hydrocarbons / oxygenates)	9	4%	34%	8
PV + EC	SnO_2/CuO	SnO_2/CuO	86.6% (CO)	11.6	13.4%	47%	9
PEC	$BiVO_4$	Cu	65% (HCOOH) at 0.75 V 80% (HCOH) at 0.9 V	0.10 0.36	0.3% (HCOOH) 0.7% (HCOH)	-	10
PV + EC	IrO_X	Nanoporous Ag	93% (CO)	6.0	8.0%	44.6%	11
PEC	TiO_2	Sn-GDE	64% (HCOOH)	2.9	0.24%	70%	12
PV + EC	IrO_2	Au	80% to 90% (CO)	5.8	6.5%	48.5%	13
PEC	$BiVO_4$/CoPi	PDA-biocathode	99% (HCOOH)	0.0001	0.042%	-	14
PEC	Fe_2O_3	BDD	62% (HCOOH)	0.28	0.3%	46%	This work

PEC: photoelectrochemical. PV: photovoltaic. EC: electrochemical. GDE: gas diffusion electrode. PDA: electrochemically synthesized polydopamine thin films.

10. References

1 Y. Ling, G. Wang, D. A. Wheeler, J. Z. Zhang and Y. Li, *Nano Lett*, 2011, **11**, 2119–2125.

2 J. Y. Kim, G. Magesh, D. H. Youn, J. W. Jang, J. Kubota, K. Domen and J. S. Lee, *Sci. Rep.*, 2013, **3**, 2681.

3 J. Y. Kim, D. H. Youn, J. H. Kim, H. G. Kim and J. S. Lee, *ACS Appl. Mater. Interfaces*, 2015, **7**, 14123–14129.

4 J. Y. Kim, D. H. Youn, K. Kang and J. S. Lee, *Angew. Chem., Int. Ed.*, 2016, **55**, 10854–10858.

5 F. Malara, A. Minguzzi, M. Marelli, S. Morandi, R. Psaro, V. Dal Santo and A. Naldoni, *ACS Catal.*, 2015, **5**, 5292–5300.

6 G. Iwai, A. Fiorani, J. Du and Y. Einaga, *Energy Adv.*, 2023, **2**, 733–738.

7 X. Zhou, R. Liu, K. Sun, Y. Chen, E. Verlage, S. A. Francis, N. S. Lewis and C. Xiang, *ACS Energy Lett.*, 2016, **1**, 764–770.

8 J. Gurudayal, D. Srankó, C. Towle, Y. Lum, M. Hettick, M. Scott, A. Javey and J. Ager, *Energy Environ. Sci.*, 2017, **10**, 2222–2230.

9 M. Schreier, F. Héroguel, L. Steier, S. Ahmad, J. Luterbacher, M. Mayer, J. Luo and M. Grätzel, *Nat. Energy*, 2017, **2**, 17087.

10 C. W. Kim, M. J. Kang, S. Ji and Y. S. Kang, *ACS Catal.*, 2018, **8**, 968–974.

11 S. Y. Chae, S. Y. Lee, S. G. Han, H. Kim, J. Ko, S. Park, O.-S. Joo, D. Kim, Y. Kang and U. Lee, *Sustainable Energy Fuels*, 2020, **4**, 199–212.

12 E. Irtem, M. D. Hernández-Alonso, A. Parra, C. Fàbrega, G. Penelas-Pérez, J. R. Morante and T. Andreu, *Electrochim. Acta*, 2017, **240**, 225–230.

13 M. Schreier, L. Curvat, F. Giordano, L. Steier, A. Abate, S. Zakeeruddin, J. Luo, M. Mayer and M. Grätzel, *Nat. Commun.*, 2015, **6**, 7326.

14 S. Y. Lee, S. Y. Lim, D. Seo, J.-Y. Lee and T. D. Chung, *Adv. Energy Mater.*, 2016, **6**, 1502207.